Journal of Orthopaedic Translation 34 (2022) 60–72

Contents lists available at ScienceDirect

Journal of Orthopaedic Translation

journal homepage: www.journals.elsevier.com/journal-of-orthopaedic-translation

Osteocyte β1 integrin loss causes low bone mass and impairs bone mechanotransduction in mice

Lei Qin [a,1], Tailin He [b,1], Dazhi Yang [a,1], Yishu Wang [b], Zhenjian Li [c], Qinnan Yan [b], Peijun Zhang [b], Zecai Chen [a], Sixiong Lin [b,d], Huanqing Gao [b], Qing Yao [b], Zhen Xu [a], Bin Tang [c], Weihong Yi [a,**], Guozhi Xiao [b,*]

[a] Department of Orthopedics, Huazhong University of Science and Technology Union Shenzhen Hospital, Shenzhen, 518000, China
[b] Department of Biochemistry, School of Medicine, Southern University of Science and Technology, Guangdong Provincial Key Laboratory of Cell Microenvironment and Disease Research, Shenzhen Key Laboratory of Cell Microenvironment, Shenzhen, 518055, China
[c] Department of Biomedical Engineering, Southern University of Science and Technology, Shenzhen, China
[d] Department of Spine Surgery, Orthopedic Research Institute, The First Affiliated Hospital of Sun Yat-sen University, Guangdong Provincial Key Laboratory of Orthopedics and Traumatology, Guangzhou, 510080, China

ARTICLE INFO

Keywords:
β1 integrin
Osteocyte
Bone homeostasis
Mechanotransduction
Collagen I

ABSTRACT

Background: The key focal adhesion protein β1 integrin plays an essential role in early skeletal development. However, roles of β1 integrin expression in osteocytes during the regulation of bone homeostasis and mechanotransduction are incompletely understood.

Materials and methods: To study the in vivo function of osteocyte β1 integrin in bone, we utilized the 10-kb *Dmp1 (Dentin matrix acidic phosphoprotein 1)-Cre* to generate mice with β1 integrin deletion in this cell type. Microcomputerized tomography, bone histomorphometry and immunohistochemistry were performed to determine the effects of osteocyte β1 integrin loss on bone mass accrual and biomechanical properties. In vivo tibial loading model was applied to study the possible involvement of osteocyte β1 integrin in bone mechanotransduction.

Results: Loss of β1 integrin expression in osteocytes resulted in a severe low bone mass and impaired biomechanical properties in load-bearing long bones and spines, but not in non-weight-bearing calvariae, in mice. The loss of β1 integrin led to enlarged size of lacunar-canalicular system, abnormal cell morphology, and disorientated nuclei in osteocytes. Furthermore, β1 integrin loss caused shortening and disorientated collagen I fibers in long bones. Osteocyte β1 integrin loss did not impact the osteoclast activities, but significantly reduced the osteoblast bone formation rate and, in the meantime, enhanced the adipogenic differentiation of the bone marrow stromal cells in the bone microenvironment. In addition, tibial loading failed to accelerate the anabolic bone formation and improve collagen I fiber integrity in mutant mice.

Conclusions: Our studies demonstrate an essential role of osteocyte β1 integrin in regulating bone homeostasis and mechanotransduction.

The transnational* potential *of this article: This study reveals the regulatory roles of osteocyte β1 integrin in vivo for the maintenance of bone mass accrual, biomechanical properties, extracellular matrix integrity as well as bone mechanobiology, which defines β1 integrin a potential therapeutic target for skeletal diseases, such as osteoporosis.

1. Introduction

Focal adhesions (FAs) between cells and their environment are crucial for the migration, proliferation, survival and differentiation of cells. In skeletal tissues, the component proteins of FAs, such as Kindlin-2 and Pinch1/2, have been reported with essential functions in regulating bone development, cartilage functions, force-induced bone formation and skeletal aging process [1–5]. As the major component of FAs, integrins

* Corresponding author.
** Corresponding author.
E-mail addresses: szyiwh@163.com (W. Yi), xiaogz@sustech.edu.cn (G. Xiao).
[1] These authors equally contribute to this article.

https://doi.org/10.1016/j.jot.2022.03.008
Received 3 January 2022; Received in revised form 19 March 2022; Accepted 21 March 2022

are transmembrane heterodimers formed by α and β subunits, which have long been recognized as the major bidirectional molecular links interconnecting cells to their extracellular matrix (ECM) [6,7]. For integrin heterodimers, the extracellular domains contribute to ligand specificity and the intracellular domains are responsible for transducing signals [8]. The most commonly found subchain in integrin heterodimers is β1 integrin [9], which has been shown to be largely involved in the process of normal development, such as embryo implantation [10] and neuronal migration [11], and abnormal pathogenesis, such as tumor initiation, cancer progression [9,12] and fibrotic diseases [13]. In skeletal environment, β1 integrin, the major type I collagen-binding subchain, is reported with broad expression in multiple cell types, including bone marrow stem cells, osteoclasts, osteoblasts and osteocytes [14–18]. Published studies show that β1 integrin actively participates in the processes of bone development and functional regulation, including stem cell differentiation, articular cartilage structure and calvarial ossification [19–22]. However, roles of β1 integrin expression in osteocytes during the regulation of bone homeostasis and mechanotransduction are incompletely understood.

Osteocytes, as the most abundant and long-lived cell type in bone tissue, are the terminally differentiated cells derived from osteoblasts. For a century, the bone biology cornerstone illustrates that bone mass maintenance is a balance between bone-forming osteoblasts and bone-resorbing osteoclasts, whereas osteocytes had been considered as a "passive placeholder" in mineralized bone. With the advances of technologies for the past twenty to thirty years, recent studies demonstrate that osteocyte is an emerging multi-functional orchestrator in bone remodeling [23] through direct regulation of local calcium abundance and phosphate metabolism [24,25], indirect modulation of osteoblast and osteoclast activities [25,26]. Importantly, osteocytes have been demonstrated as the principal mechano-responsive cells in bone [19,21,27–29].

β1 integrin is one of the major integrin subunits expressed in osteocytes [19]. Studies showed that β1 integrin in osteocytes is mainly observed on the plasma membrane around cell body [30], where it forms traditional FA complex with vinculin and paxillin [31]. The involvements of β1 integrin in early skeletal development have been well documented, including the survival of mesenchymal stem cells [18], mesenchymal condensation [32], chondrocyte maturation [22] and pre-osteoblast functions [32]. In contrast, roles of β1 integrin in mature osteoblasts and osteocytes have less been established and even appeared to be controversial. For example, deleting β1 integrin expression using the *Osteocalcin-Cre*, which primarily targets differentiated osteoblasts and osteocytes, caused no effects in the bone mineral density, biomechanics or fracture healing, but only minor femur structure alternations in 12-week-old mice [32]. However, overexpression of a domain-negative form of β1 integrin subunit (β1 integrin-DN) under the same *Osteocalcin* promoter led to reduced bone mass, increased cortical porosity in long bones and thinner skull flat bones in transgenic animals [33].

In this study, we demonstrate that mice with β1 integrin deletion in osteocytes display severe osteopenia and fail to increase bone formation by mechanical loading. Osteocyte β1 integrin loss did not impact the osteoclast formation, but significantly reduced the osteoblast bone formation rate and, in the meantime, enhanced the adipogenic differentiation of the bone marrow stromal cells in the bone microenvironment. We demonstrate that osteocyte β1 integrin regulates bone homeostasis through both cell-autonomous and non-cell-autonomous mechanisms.

2. Materials and methods

2.1. Animal study

Floxed *Itgβ1* mice ($Itg\beta1^{f/f}$) were purchased from Jackson Laboratory (Stock No: 004605) with the *loxP* sites flanking exon 3 of the *Itgβ1* gene. Mice with 10-kb mouse *Dmp1* gene promoter-driving Cre recombinase expression (*Dmp1-Cre*) were generated as described in Ref. [34]. Mice with conditional deletion of *Itgβ1* (*Dmp1-Cre; Itgβ1*$^{f/f}$, referred to as cKO hereinafter) were generated by inter-crossing heterozygote male mice (*Dmp1-Cre; Itgβ1*$^{f/+}$) with homozygous female mice ($Itg\beta1^{f/f}$) mice. In this study, age- and gender-matched Cre-negative littermates ($Itg\beta1^{f/f}$) were used as control mice in each experiment. Primers used for mouse genotyping were listed in Table 1. All research protocols were approved by the Institutional Animal Care and Use Committee (IACUC) of Southern University of Science and Technology. All relevant guidelines for the work with animals were adhered to in this study.

2.2. Mouse tail DNA extraction and genotyping

Experimental mice were weaned at day of postnatal 21, with a small bit of tail tissue collected. Mouse genome DNAs were extracted from tail tissue with Quick Genotyping Assay Kit (Beyotime, Cat# D7283M) following the manufacturer's protocol. PCR and agar gel examination were performed for mouse genotyping by using the PCR primers for *Dmp1-Cre* and *β1 integrin* sequences as listed in Table 1.

2.3. Micro-computerized tomography (μCT)

Either live anesthetized mice or fixed non-demineralized bones were subjected to μCT analyses in the Southern University of Science and Technology using a Bruker μCT (SkyScan 1172 Micro-CT, Bruker Micro-CT, Kontich, Belgium) as described before [35]. The parameters for cortical bone include the bone mineral density (BMD, g/cm^3), bone volume fraction (BV/TV) and cortical thickness (Ct.Th, mm). The parameters for trabecular bone include BMD, BV/TV, trabecular thickness (Tb.Th, μm), trabecular separation (Tb.Sp, μm) and trabecular number (Tb.N, 1/mm). Tibial parameters were assessed at the proximal spongiosa from the end of growth plate to 0.75 mm extending distally for trabecular bone, 0.5 mm length of mid-shaft tibia for cortical bone. Femur trabecular bone parameters were assessed from the distal growth plate to 1.0 mm extending proximally; cortical bone parameters were determined from 1.0 mm length of mid-shaft femur. The whole head was scanned with the calvarial region-of-interest (ROI) set at the center of skull with 2 mm × 2 mm size. The lumbar spines were dissected and scanned from L3 to L5. Detailed μCT analyses of spine trabecular bone parameters were assessed from the proximal growth plate to the distal growth plate in the L4 lumbar spines.

2.4. Femur three-point bending

The three-point bending test was conducted with ElectroForce (Bose ElectroFore 3200; EndureTEC Minnetonka, MN, USA) as previously described [35]. Briefly, femurs were dissected free of soft tissue and immediately kept in 1xPBS at 4 °C before bending test. The strength test was performed at the mid-shaft of femurs with continuous displacement of 0.05 mm/s in a single stop setting (ramp waveform, span length, 7 mm). Whole femur mechanical properties, including maximum load, maximum displacement, stiffness and work-to-fracture were determined using load–displacement diagrams.

Table 1
Mouse genotyping PCR sequences.

Name	5′ primer	3′ primer
Cre	GATCTCCGGTATTGAAACTCCAGC	GCTAAACATGCTTCATCGTCGG
Itgβ1	CGGCTCAAAGCAGAGTGTCAGTC	CCACAACTTTCCCAGTTAGCTCTC

2.5. In vivo tibial loading

Force loading experiments were conducted as previously described in Ref. [35] using an electro actuator (Bose ElectroFore 3200; EndureTEC Minnetonka, MN, USA). Briefly, mice were under anesthesia with 2.5% Avertin injection (100 μl per 10 g body weight). The right tibia was cyclically loaded with axial compression force (triangular waveform, 4 Hz, 9.0 N peak force, 1200 cycles per loading). The left limbs were kept intact and served as unload internal controls. Mice were loaded on alternative day for two weeks. Injection of calcein (30 mg/kg body weight; Sigma, Saint Louis, MO, USA) was administered at Day 4 and Day 12, respectively. Animals were sacrificed two weeks (Day 14) after experiments for bone histomorphometry.

2.6. Bone histology and immunohistochemistry

For double calcein labeling experiments, bone samples were embedded in methyl methacrylate following the manufactory plastic embedding protocol (EM0200, Osteo-Bed Bone Embedding Kit, Sigma, MO, USA) as described in Ref. [1]. Transverse sections of 6 μm thickness of bone samples were cut with an annular diamond saw. Images of double calcein labeling bone sections were visualized using the argon 488 nm laser of fluorescent microscopy (Olympus, BX53). The mineral apposition rate (MAR) was calculated as the average distance between the double calcein labels divided by the number of the days between the two calcein injections. The mineralizing surface per bone surface (MS/BS) was calculated as $MS/BS = (dLS + sLS/2)/BS$, where dLS is the total length of double-labeled surfaces and sLS is the total length of single-labeled surfaces. The bone formation rate per bone surface (BFR/BS) is the volume of mineralized bone formed per unit time and per unit bone surface, calculated as $BFR/BS = MAR \times (MS/BS)$.

For bone immunohistochemistry (IHC) and immunofluorescence (IF), bone samples were decalcified with 10% ethylenedinitrilotetraacetic acid (EDTA, Sigma) for 2–3 weeks. Samples were embedded in paraffin and cut in 5 μm thickness sections. IHC and IF experiments were performed using our standard protocols as previously described in Refs. [36,37]. Collagen staining and concentration detection were performed with sirius red/fast green collagen staining kit (Chondrex, Inc, Woodinville, WA, USA cat#: 9046) following the manufacturer staining and extraction protocol. F-actin cytoskeleton staining was conducted on tibial cryosections stained with Rhodamine-Phalloidin dye (Thermo Fisher, Alexa Fluor™ 488, Cat# A12379). For lacunar-canalicular system (LCS) staining, bone samples were collected and treated as described in Ref. [38]. In general, tibia bone blocks were pre-stained with FITC solution (10%, diluted in 100% ethanol; Thermo Fisher, Alexa Fluor™ 488, Cat# A10235) for 2 days, then embedded for frozen section and cut into 10 μm thickness for direct confocal imaging. Antibodies used in this study are listed in Table 2.

2.7. Serum ELISA

Serum samples were collected from the supernatant of centrifuged (4 °C, 12000g, 20 min) mouse whole blood after coagulation for 1 h at room temperature. Samples were immediately kept at −80 °C fridge before usage. Serum levels of P1NP and CTX-1 were measured by ELISA kits, i.e., IDS Rat/Mouse PINP EIA kit and The RatLaps™ (CTX-I) EIA assay (Immunodiagnostic Systems Limited, 10 Didcot Way, Boldon Business Park, Boldon, Tyne & Wear, NE35 9PD, UK).

Table 2
Antibodies information.

Name	Supplier	Cat #	Western blot usage	IF/IHC usage
β1 Integrin	Cell Signaling	#34971	1:1000	
β1 Integrin	Abcam	Ab95623		1:200
β3 Integrin	Cell Signaling	#13166	1:1000	
Kindlin-2	Millipore	MAB2167	1:1000	
Perilipin	Cell Signaling	#3470		1:200
Gapdh	Abcam	Ab245355	1:1000	

2.8. Immunofluorescence, confocal imaging and two-photon imaging

Immunofluorescence staining with paraffin samples were conducted as described in Refs. [39,40]. Specifically, paraffin bone samples were cut in 5 μm thickness, followed by standard re-hydration process, penetrated with 0.25% Triton X-100, blocked with 1% BSA and then incubated with antibodies. Antibodies used in this study are listed in Table 2. Confocal images were conducted by Nikon A1R laser-scanning confocal microscopy with 0.5 μm z-stack interval. Second-harmonic generation (SHG) and two-photon excited fluorescence imaging were conducted to investigate collagen fibers with inverted two-photon Olympus FVMPE-RS microscopy.

2.9. Quantitative real-time PCR and western blotting analyses

Protein and mRNA samples from long bone tissues, i.e. tibiae and femurs, were dissected free of muscle or other soft tissues, flashed out the bone marrow and only kept osteocyte-enriched cortical bones. The procedure for qPCR and western blotting experiments were conducted as described in Refs. [41,42]. Generally total RNA was extracted from cultured cells and bone samples using Trizol reagents. Synthesis of cDNA was performed using 2 μg of RNA by a Transcriptor First Strand cDNA Synthesis Kit according to the manufacturer's instructions. Relative mRNA expression levels were determined using a SYBR Green qPCR kit with CFX96 Real-Time System. *Gapdh* mRNA was used for normalization. The specific primers for gene expression analysis were listed in Table 3. For western blotting, cell lysates and bone samples were harvested in RIPA lysis buffer. Protein concentration was measured with a BCA kit. Aliquots of 20 μg total protein were separated and transferred onto a PVDF membranes. Membranes were blocked at room temperature in 5% non-fat powdered milk for 1 h, followed by an overnight incubation at 4 °C with primary antibodies. The specific primary antibodies for western blotting were listed in Table 2. After incubation with appropriate HRP-conjugated secondary antibodies, blots were developed using an enhanced chemiluminescence and exposed in ChemiDoc XRS chemiluminescence imaging system.

2.10. Nano-indentation

The nano-indentation experiments were performed as described in Ref. [35] with a Nano Indenter G200 (Keysight Technologies, Inc, Santa Rosa, CA, USA), equipped with a three-sided pyramid Berkovich diamond tip. Briefly, the identical loading scheme applied consists of a loading stage at a constant rate of 20 mN/min to a depth of 1000 nm, holding at this load for a period of 10 s and then unloading to 15% of the peak load at a rate of 10 mN/min. Each sample was performed for twenty indentations at the midshaft of bone samples. For the indenter tip,

Table 3
Mouse quantitative real-time PCR primers.

Name	5′ primer	3′ primer
Gapdh	CAGTGCCAGCCTCGTCCCGTAGA	CTGCAAATGGCAGCCCTGGTGAC
Colla1	GCTCCTCTTAGGGGCCACT	CCACGTCTCACCATTGGGG
Runx2	AACGATCTGAGATTTGTGGGC	CCTGCGTGGGATTTCTTGGTT
Sp7	ATGGCGTCCTCTCTGCTTG	TGAAAGGTCAGCGTATGGCTT
Bglap	AGGGAGGATCAAGTCCCG	GAACAGACTCCGGCGCTA
Cebpα	CAAGAACAGCAACGAGTACCG	GTCACTGGTCAACTCCAGCAC
Cebpβ	CAAGCTGAGCGACGAGTACA	CAGCTGCTCCACCTTCTTCT
Ap2	GGGGCCAGGCTTCTATTCC	GGAGCTGGGTTAGGTATGGG
Pref-1	CCCAGGTGAGCTTCGAGTG	GGAGAGGGGTACTCTTGTTGAG
Adiponectin	TGTTCCTCTTAATCCTGCCCA	CCAACCTGCACAAGTTCCCTT
Pparγ	TCGCTGATGCACTGCCTATG	GAGAGGTCCACAGAGCTGATT

Young's modulus (Ei) = 1140 GPa and Poisson's ratio (vi) = 0.07. The Poisson ratio for bone is set at 0.3 for calculating the modulus values.

2.11. In vitro bone marrow stromal cells (BMSCs) culture and differentiation

Mouse primary BMSCs were isolated from both femurs and tibiae and cultured as described previously [43]. For osteogenic differentiation, BMSCs were cultured in osteogenic medium (α-MEM containing 10% FBS and 50 μg/mL ascorbic acid) for 7 days and then stained for ALP using a BCIP/NBT ALP color development kit (Beyotime, China). BMSCs were differentiated in osteogenic medium for 14 days for alizarin red S staining using Alizarin Red S Staining Kit (Beyotime, China) and qPCR analysis. For adipogenic differentiation, BMSCs were cultured with reagents from the MesenCult™ Adipogenic Differentiation Kit (Stemcell Technologies) for 9 days and then stained with Oil red O (Sigma) and qPCR analysis.

2.12. Statistical analysis

All data were analyzed in this study by using the GraphPad Prism software (Version 8.0). The differences between two groups were analyzed by unpaired two-tailed Student's *t*-test. Results are expressed as mean ± standard deviation (s.d.). Difference with $p < 0.05$ was considered as statistically significant. All experiments were repeated at least three times.

3. Results

3.1. Deletion of β1 integrin in osteocytes causes low bone mass in the weight-bearing bones of adult mice

To determine the in vivo roles of β1 integrin in osteocytes, we generated osteocytes-specific β1 integrin deletion mice (hereinafter referred to as $Itg\beta1^{Dmp1}$ or conditional knock-out or cKO) by breading the floxed *Itgβ1* mice ($Itg\beta1^{f/f}$) with the 10-kb mouse *Dmp1 (dentin matrix acidic phosphoprotein 1)-Cre* transgenic mice [34]. The deletion of β1 integrin was confirmed by PCR genotyping using mouse tail DNAs (Supplementary Fig. 1a) and western blotting of osteocyte-enriched cortical bone tissues (Fig. 1a and b) and immunohistochemistry (IHC) with the cortical bone sections of tibiae from control ($Itg\beta1^{f/f}$) and cKO ($Itg\beta1^{Dmp1}$) mice (Fig. 1c). Compared to the cortical bone samples, the expression levels of β1 integrin in other organs, such as heart, kidney, lung, spleen and liver were indistinguishable between control and cKO mice (Supplementary. Fig. 1b). cKO mice exhibited indistinguishable body weight, and similar body structure compared to their age- and sex-matched control mice during development (Supplementary. Fig. 1c and d). Likewise, there were no differences in the length of femurs and tibiae between the two genotypes (Supplementary. Fig. 1e–h).

Detailed analysis of potential skeletal phenotypes of control and cKO mice were examined through high resolution micro-CT (μCT) at 4-month age when their skeletons were matured. We detected the bone mass from the mid-shaft cortical bone of femurs and tibiae, the distal trabecular bone of femurs, and the proximal trabecular bone of tibiae from male control and cKO mice (Fig. 1d, h). Compared with their age- and sex-matched controls, cKO mice showed an 44.7% increase in trabecular separation (Tb. Sp) and a 39.9% reduction in trabecular number (Tb. N) of femurs (Fig. 1e and f). These numbers went to 56.0% increase in Tb. Sp and 52.5% reduction in Tb. N for the tibiae of cKO mice (Fig. 1i and j). Importantly, the cortical thickness (Ct.Th) of femurs and tibiae from cKO mice significantly dropped 8.5% and 5.3% compared to the control mice, respectively (Fig. 1g, k). In line with these observations, the bone volume fraction (BV/TV) and the relative intensity of mineralized bone at the spine (L3 to L5) of cKO mice were significantly reduced compared to those in control mice (Fig. 1l–o). Similar with these observations in male mice, cKO female mice also displayed a similar osteopenia in tibiae with a 24.2% reduction in trabecular BV/TV and a 23.2% reduction in Tb. N (Supplementary Figs. 2a–c). However, the cortical thickness of tibiae was comparable between control and cKO female mice at 4-month age (Supplementary Fig. 2d). Detailed bone parameters from μCT analyses for male femurs, male tibiae, male spines and female tibiae were listed in Supplementary Fig. 3.

We next determined the potential impact of β1 integrin loss in osteocytes on calvariae, which are non-weight-bearing bones, by comparing the bone mass and structure of calvariae from the two genotypes. The overall skull size, structure and shape were comparable between control and cKO mice (Supplementary Fig. 4a e, f). A region-of-interest (ROI) analysis of the 2 mm × 2 mm center in the skull showed that control and cKO mice shared similar bone mineral density (BMD), BV/TV and skull thickness (Supplementary Figs. 4b–d).

Collectively, these results demonstrate that deletion of β1 integrin in osteocytes causes a severe osteopenia in femurs, tibiae and spines, all weight-bearing long bones.

3.2. β1 integrin loss in osteocytes impairs multiple mechanical properties with collagen I fiber disorientation in long bones

Besides bone mass, the mechanical property of bones is another important parameter that defines bone health. Wondering whether β1 integrin in osteocytes participates in bone quality control, we challenged the femurs from 4-month-old male mice with three-point-bending test. As presented in the load–displacement curve (Fig. 2a), femurs from control mice resisted to significantly higher bending forces with larger displacement before bone fracture, compared to those from cKO mice. Statistically, the average maximum load of control femurs (18.35 ± 2.30 N) were 2.63 ± 0.75 N higher than that of cKO femurs (15.72 ± 1.49 N) (Fig. 2b). The average stiffness of control femurs was 140.0 ± 5.44 N/mm; this number was dropped to 116.80 ± 4.99 N/mm of cKO femurs (Fig. 2c). Moreover, the average fracture energy (work-to-fracture) for control femurs was significantly higher in control mice (7.51 ± 0.40 N mm) than that for cKO femurs (4.29 ± 0.37 N mm) (Fig. 2d). In consistence with these observations from male mice, the three-point-bending results from female mice also presented clear reduction of bone mechanical properties in cKO femurs (Supplementary Figs. 2e–h). Collectively, these results demonstrate that osteocyte β1 integrin actively participates in the maintenance of bone mechanical properties.

Bone samples are generally defined with two mechanical properties, elastic modulus and hardness [44]. The elastic modulus, often known as Young's modulus, is an intrinsic material property of bone which is related to the resistance offered by the bone to elastic deformations. Hardness is an engineering property in characterization of bone microstructures and its resistance to penetration, which has been shown with great associations to bone matrix composition, such as collagen fibers [45,46]. To further examine the bone mechanical properties of the two genotypes in nano- and micro-scale, we applied the nanoindentation approach to evaluate both Young's modulus and hardness of non-decalcified tibial samples from control and cKO male mice (Fig. 2e and f). We analyzed the center region of tibial middle-shaft cortical bone sections. Interestingly, we found that the average Young's modulus was comparable between control (9.15 ± 0.63 GPa) and cKO tibiae (8.88 ± 0.69 GPa) with a slight drop in cKO mice. However, the hardness of cKO tibiae (0.177 ± 0.03 GPa) was dramatically reduced by 60.4% compared to that of control tibiae (0.447 ± 0.04 GPa).

Published studies suggest that the contents of bone matrix, especially type I collagen, which accounts for 90% of the bone matrix proteins, in the cortical bones influence the bone strength [47]. The maturation and orientations of collagen fibers, as well as their interactions with bone mineral together determinate bone quality. To test whether collagen matrix was altered after β1 integrin loss in osteocytes, we visualized and semi-quantitatively measured the collagen content on the sagittal tibial sections from control and cKO mice with sirius red/fast green dye staining (Fig. 2g–j). In this staining, sirius red specifically binds the

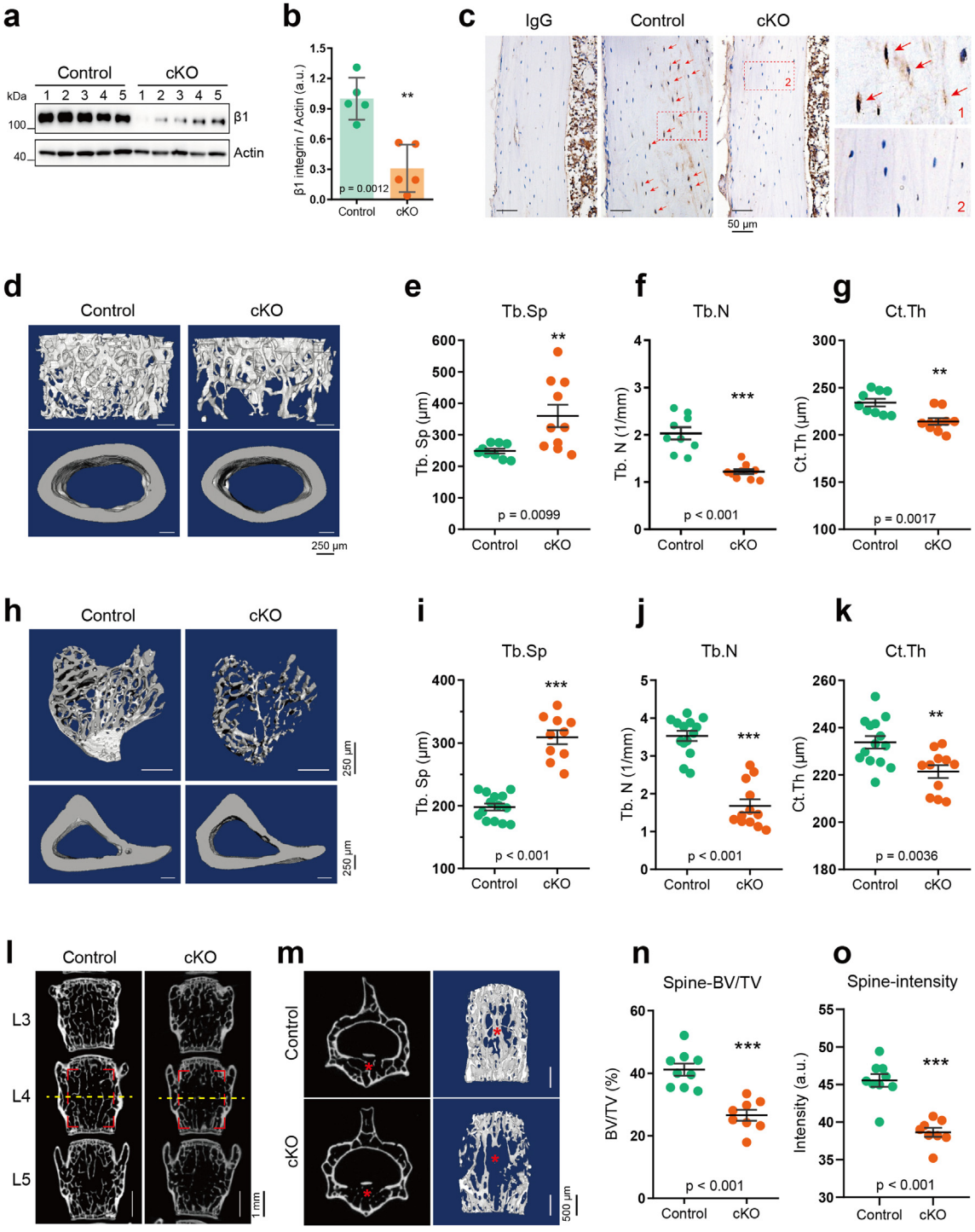

Figure 1. β1 integrin deletion in osteocytes results in significant bone loss in weight-bearing long bones in adult mice (**a**–**b**) Western blotting results of cortical bone samples from control and cKO mice. Protein extracts were isolated from osteocyte-enriched cortical bone tissues and subjected to western blotting for the expression analyses of β1 integrin. α-actin was used as a loading control. (**c**) Immunohistochemistry (IHC) of the tibial cortical bone sections from control and cKO mice. (**d**) Micro-computerized tomography (μCT) images of the distal trabecular bone and mid-shaft cortical bone of femurs from 4-month-old male control and cKO mice (**e**–**g**) Quantitative μCT analyses of trabecular separation (Tb.Sp), trabecular number (Tb.N), and cortical thickness (Ct.Th) of femurs. $N = 9$ for control group and $N = 10$ for cKO group. (**h**) μCT images of the proximal trabecular bone and mid-shaft cortical bone of tibiae from 4-month-old male control and cKO mice (**i-k**) Quantitative μCT analyses of Tb. Sp, Tb.N, and Ct. Th of tibiae. $N = 14$ for control group and $N = 10$–12 for cKO group. (**l**) μCT images of the sagittal view of L3-5 lumbar spines from 4-month-old male control and cKO mice. (**m**) Cross-section images (at yellow dotted line in **l**) and 3D reconstruction images (at red square ROI in **l**) of the L4 lumbar spines from control and cKO mice (**n**–**o**) Quantitative μCT analyses of the bone volume/tissue volume (BV/TV) and arbitrary intensity of spine sections from control and cKO mice. $N = 9$ for control group and $N = 8$ for cKO group. Results are expressed as mean ± standard deviation (s.d.). $^{**}p < 0.01$; $^{***}p < 0.001$.

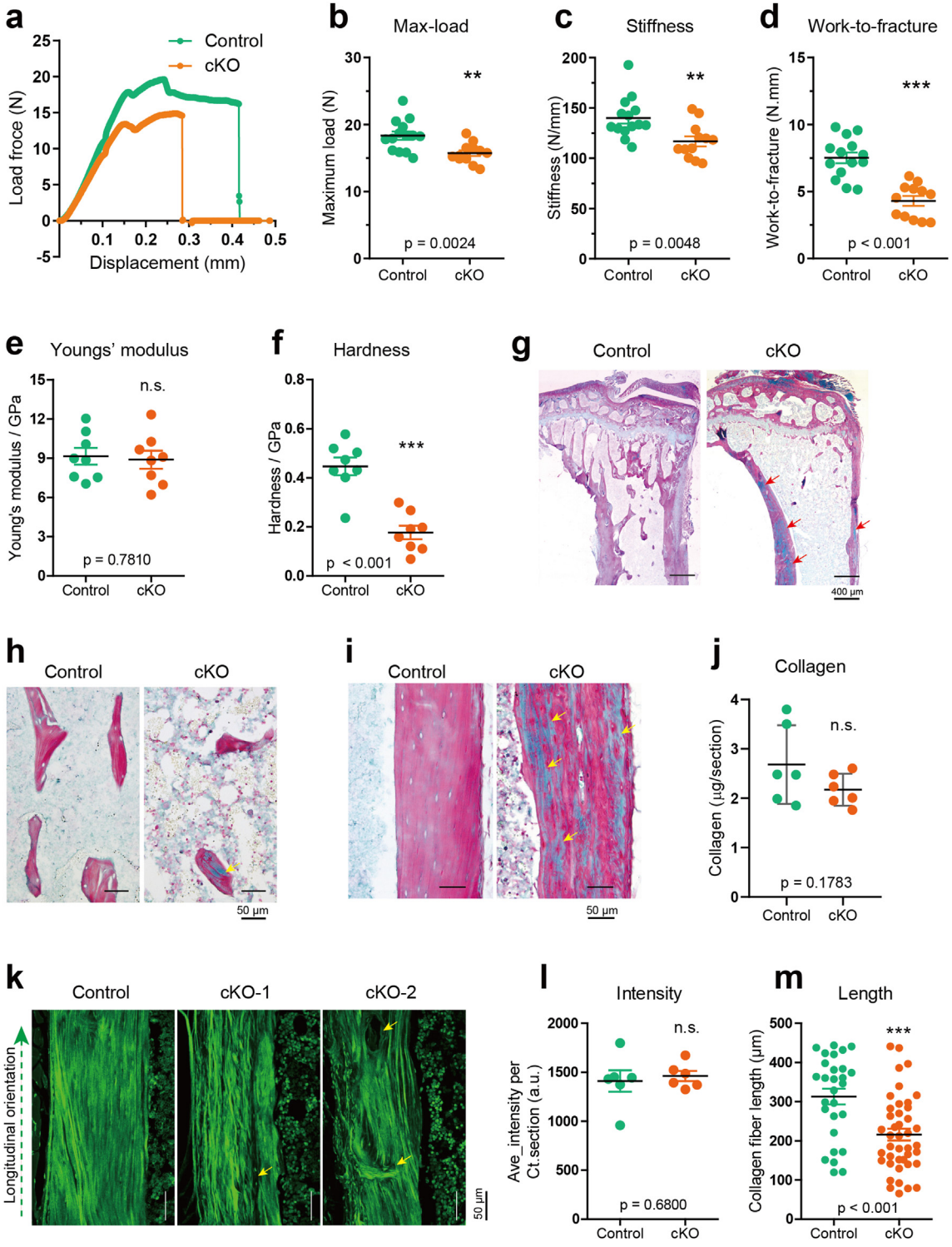

Figure 2. β1 integrin loss impairs bone mechanical properties and alters collagen fiber integrity. (**a**) Representative load–displacement curve from three-point-bending (3 PB) test in 4-month-old male control and cKO mice (**b–d**) Quantitative analyses of maximum load force (Max-load), stiffness and work-to-fracture in 3 PB test. $N = 14$ for control group and $N = 12$ for cKO group (**e–f**) Quantitative analyses of Young's modulus and hardness for 4-month-old male control and cKO mice in nanoindentation test. $N = 8$ for each group (**g–i**) Sirius red/fast green dye staining of tibial sections from 4-month-old male control and cKO mice (**j**) Semi-quantitative measurement of the collagen content on the sagittal tibial sections from control and cKO mice. $N = 6$ for each group (**k**) Representative images of collagen fibers under two-photon microscopy from 4-month-old male control and cKO tibial sections (**l–m**) Quantitative analyses of collagen fiber intensity and length for control and cKO mice. $N = 6$ for each group. Results are expressed as mean ± standard deviation (s.d.). n. s. $p > 0.05$; *$p < 0.05$; **$p < 0.01$; ***$p < 0.001$.

[Gly-X-Y]n helical structure of fibrillar collagens, whereas fast green binds to non-collagenous proteins. Since the cortical bone mainly contains type I collagen in the matrix, we visualized the collagen I with sirius red dye staining. As shown in Fig. 2g, the red staining of collagen I was relatively uniformed throughout the sections of control tibiae, but was discontinuous with some disrupted non-collagenous proteins detected in the middle of cKO tibiae (red arrows in Fig. 2g). These observations could be found under higher magnification microscopy. In both trabecular bone (Fig. 2h) and cortical bone (Fig. 2i), we visualized continous collagen I fibers in control tibiae, but disrupted collagen I fibers coupled with non-collagen proteins in cKO tibiae (yellow arrows in cKO sections). We also semi-quantified the amount of collagen in these bone sections and found that collagen content was only slightly, but not significantly, reduced in cKO mice relative to that in control mice (Fig. 2j).

To further confirm the changes of collagen I fibers in cKO bone, we applied second-harmonic-generation (SHG) microscopy with two-photon excited fluorescence imaging to in vivo visualize fibrillar collagen fibers [48]. As collagen I is the primary matrix constituent responsible for SHG signals in cortical bone section, we were able to visualize the fiber intensity, fiber length and orientation in the sagittal sections of both control and cKO tibiae. As shown in Fig. 2k, control tibiae displayed highly oriented collagen I fibers, most of which were well aligned in the longitudinal direction in which the tibiae experience the majority of mechanical load. In contrast, cKO tibiae showed either non-uniformed fiber orientation with some gaps between different fibers (yellow arrows in cKO-1 of Fig. 2k), or dis-orientated fibers, such as transverse fibers (yellow arrows in cKO-2 of Fig. 2k). When we compared the arbitrary intensity from collagen fibers between control and cKO tibial sections (Fig. 2l), we found that the average intensity of collagen fibers from 10 μm thickness sections were similar between two groups. This data suggests that β1 integrin loss in osteocytes causes no or little reduction of collagen I fiber content in bone, which was consistent with previous semi-quantitative collagen concentration detection (Fig. 2j). However, after manually tracking the single fiber length in tibial sections, we observed a dramatic shortening of collagen fibers in cKO mice (Fig. 2m).

Collectively, these results demonstrate that loss of β1 integrin in osteocytes reduces both bone mass and bone quality of load-bearing long bones in mice. The reduction of bone hardness in cKO mice could be a consequence of the shortening and disorientation of collagen I fibers in long bones.

3.3. β1 integrin loss in osteocytes alters lacunar-canalicular size, cellular morphology, and nuclear orientation

With above observations on the bone quantity and quality changes in cKO mice, we further analyzed the possible cell-autonomous defects of osteocytes after β1 integrin deletion. We first compared the number of osteocytes in both trabecular bones and cortical bones between the two genotypes. As shown in Fig. 3a–d, the average osteocyte numbers in the sections of tibial trabecular bones and cortical bones were similar between control and cKO mice, which suggests that the reduced bone mass and quality are not a result of cell loss. Results from the hematoxylin and eosin (H/E) staining showed that the lacunar size surrounding osteocytes in cKO bones appeared to be larger than that in control bones (red arrows in cKO section of Fig. 3c). Next, we stained the lacunar-canalicular system (LCS) and actin cytoskeleton of osteocytes from the sagittal cryosections of tibiae, and quantified the related parameters under confocal microscopy with higher magnifications. As shown in Fig. 3e, compared to control mice, the lacuna from cKO mice had larger but less uniformed size (Fig. 3f) with a higher roundness score (Fig. 3g). Consistent with LCS detection, we also observed rounder and more disorientated osteocytes in cKO tibial sections. As shown in Fig. 3h, control osteocytes displayed a typical spindle-like cell body with complex and out-reaching actin-enriched processes (also see zoom-in image #1 in Fig. 3h). However, cKO osteocytes had rounder cell body with less and shorter processes (also see zoom-in image #2 in Fig. 3h). Statistical data showed that the average length of actin-enriched processes dropped 40.6% (Fig. 3i), and that the number of processes per osteocyte dropped 42.1% (Fig. 3j) after β1 integrin deletion. Moreover, results from western blotting showed significant reductions in the expression of other FA proteins, including β3 integrin and Kindlin-2, in cKO cortical bone samples (Fig. 3k and l).

From above staining images, we noticed a clear nuclear size and orientation changes in cKO sections (Fig. 3h). We next quantified the osteocyte nuclear size and roundness, and found significant alternations of nuclear size (Fig. 3n) and shape (Fig. 3o) in β1 integrin deleted osteocytes. Furthermore, analysis focused on nuclear orientation showed that the majority of control osteocytes (80.2%) displayed a longitudinal orientation (angle-α within 0–30°) (Fig. 3m, p). However, in cKO osteocytes, there were increasing numbers of osteocytes that orientated in a transverse way (angle-β larger than 30°) (Fig. 3m, p). Statically, the average nuclear angle was increased 9.3 ± 2.20° (16.88° for angle-α in control osteocytes compared to 26.19° for angle-β in cKO osteocytes) after β1 integrin was deleted (Fig. 3p).

Together these results suggest that β1 integrin controls osteocytes' autonomous functions, including LCS size and roundness, process length and density, and their nuclear size, shape and orientations.

3.4. β1 integrin loss reduces bone formation without affecting osteoclast activities

To test the non-cell-autonomous effects of β1 integrin deletion in osteocytes, we next analyzed the number and activity of the other two important bone cells, i.e., osteoclasts and osteoblasts, in control and cKO mice. We performed tartrate-resistant acid phosphatase (TRAP) staining on tibial sections from the two genotypes (Fig. 4a). We found that the osteoclast surface/bone surface and osteoclast number were comparable between 4-month-old male cKO mice and their control littermates (Fig. 4b and c). To test the in vivo osteoclast activity, we measured the serum levels of collagen type I cross-linked C-telopeptide (CTX-1), an in vivo indicator of osteoclast-mediated bone resorbing activity, and found that there was no significant difference of the serum CTX-1 levels between the two genotypes (Fig. 4d). Thus, β1 integrin loss in osteocytes seems not to affect the number and the bone-resorbing activity of osteoclasts.

We next traced the bone formation activity of osteoblasts in control and cKO long bones. We conducted double calcein labeling to measure the in vivo bone-forming activity of osteoblasts and found significant decreases in the mineral apposition rate (MAR) and a clear drop in the mineralizing surface per bone surface (MS/BS) of the metaphyseal trabecular bones (Tb) and mid-shaft cortical bones (Cb) in 4-month-old male cKO mice compared to their control littermates (Fig. 4e–g). We also measured the level of serum procollagen type 1 N-terminal propeptide (P1NP), a serum indicator of in vivo osteoblast function and bone formation, and observed a clear reduction of P1NP in the serum of cKO mice compared to that in control littermates (Fig. 4h).

We next collected the bone marrow stromal cells (BMSCs) from control and cKO mice and conducted in vitro osteogenic differentiation assays with these BMSCs. During BMSC collection and culture, we noticed that the total BMSC numbers and their in vitro doubling speed were indistinguishable between control and cKO cultures. To detect the ability of BMSCs in early stage osteogenic differentiation, we cultured BMSCs from both genotypes with osteogenic medium for 7 days and detected a significant reduction of alkaline phosphatase (ALP) activity in cKO BMSC cultures relative to that in control BMSC cultures (Fig. 4i and j). We also extended the osteogenic induction period to 14 days and conducted alizarin red S staining and quantitative PCR (qPCR) experiments to test the ability of BMSCs for late stage osteogenic differentiation. Alizarin red S staining is a commonly used method for visualizing

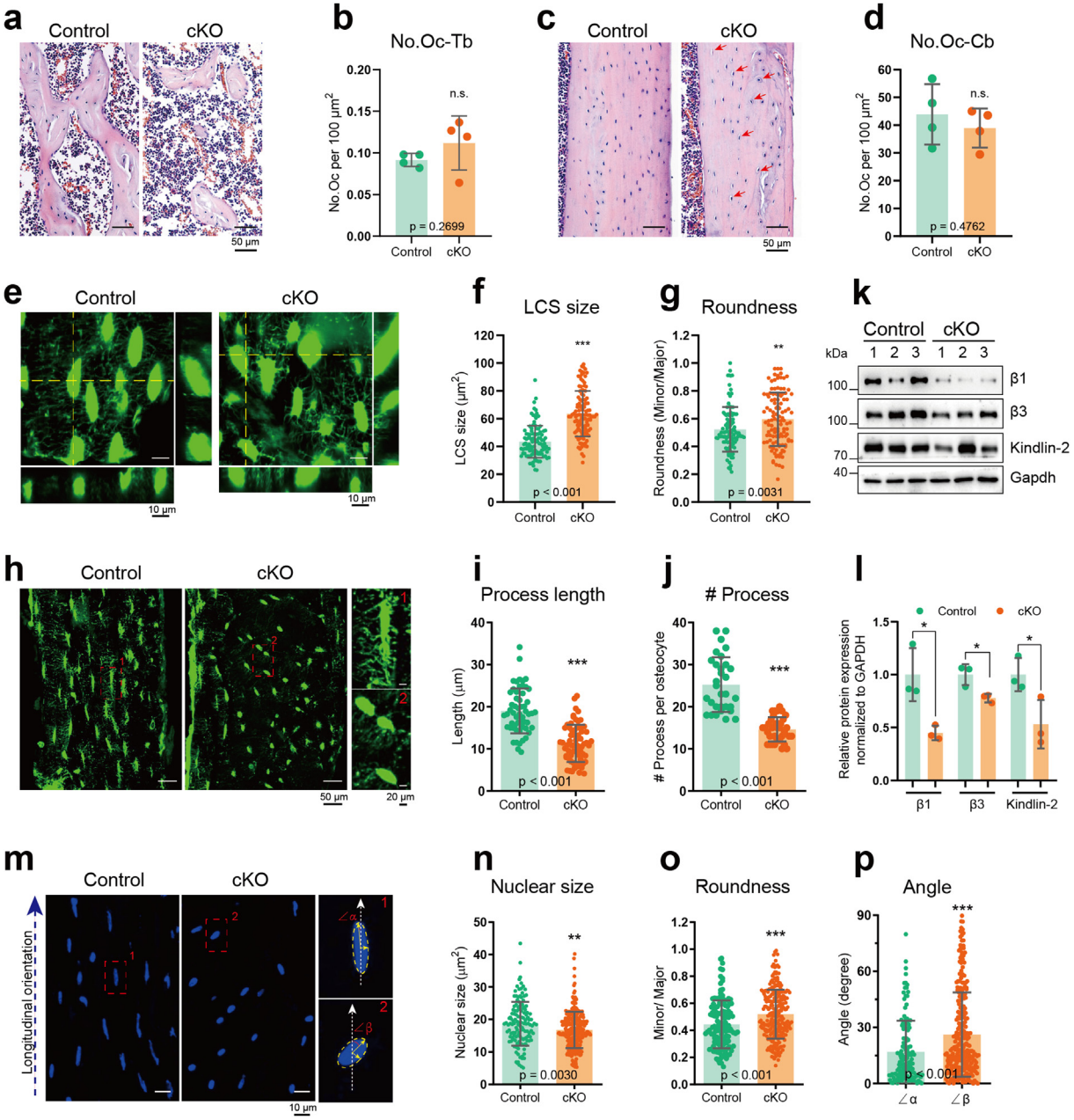

Figure 3. β1 integrin loss alters lacunar-canalicular (LCS) size, cellular morphology and nuclear orientation in osteocytes (**a**, **c**) H/E staining results of trabecular and cortical sections from 4-month-old male control and cKO tibiae (**b**, **d**) Quantitative analyses of trabecular and cortical osteocyte numbers per 100 μm^2 area in tibial sections. (**e**) Representative LCS images from the cortical tibial sections of 4-month-old male control and cKO mice (**f**–**g**) Quantitative analyses of size and roundness of LCS in control and cKO mice. (**h**) Representative actin cytoskeleton images from Rhodamine-Phalloidin staining of the cortical tibial sections from 4-month-old male control and cKO mice. Zoom-in images of #1 and #2 represent control and cKO osteocyte actin cytoskeleton, respectively (**i**–**j**) Quantitative analyses of cortical osteocyte process length and number for control and cKO mice (**k**, **l**) Western blotting results and quantifications for β1 integrin, β3 integrin, Kindlin-2 and Gapdh expression from osteocyte-enriched cortical bone samples of control and cKO mice (**m**) Representative images for osteocyte nuclei from the cortical tibial sections of 4-month-old male control and cKO mice. Zoom-in images of #1 and #2 represent the angle α and β, respectively, i.e., angles between longitudinal direction of tibia sections and major axis of control and cKO nuclei (**n**–**p**) Quantitative analyses of nuclear size, nuclear roundness, and angle α/β from control and cKO cortical osteocytes. Results were collected from three biological replicates ($N = 3$) for each group. Results are expressed as mean ± standard deviation (s.d.). n. s. $p > 0.05$; *$p < 0.05$; **$p < 0.01$; ***$p < 0.001$.

the calcium mineral deposition in culture and bone tissue. We found that BMSCs derived from control mice had more positive staining with larger calcium deposits in culture dishes than that of cKO mice (Supplementary Fig. 5). Moreover, we further showed that the expression of osteoblast-specific markers, including those encoding collagen type I alpha 1 chain (Collα1), runt-related transcription factor 2 (Runx2), Sp7/Osterix and Bglap/Osteocalcin, were significantly reduced in cKO BMSC cultures (Fig. 4k).

3.5. *Loss of β1 integrin in osteocytes enhances BMSC adipogenic differentiation in vitro and in bone*

Since BMSC can differentiate into osteoblast-lineage cells and adipocytes in bone, we wondered whether their adipogenic differentiation is affected in cKO mice. We determined the adipogenic differentiation capability of collected BMSCs with both Oil red O staining and qPCR analysis. After 9 days' adipogenic induction, we observed an obvious

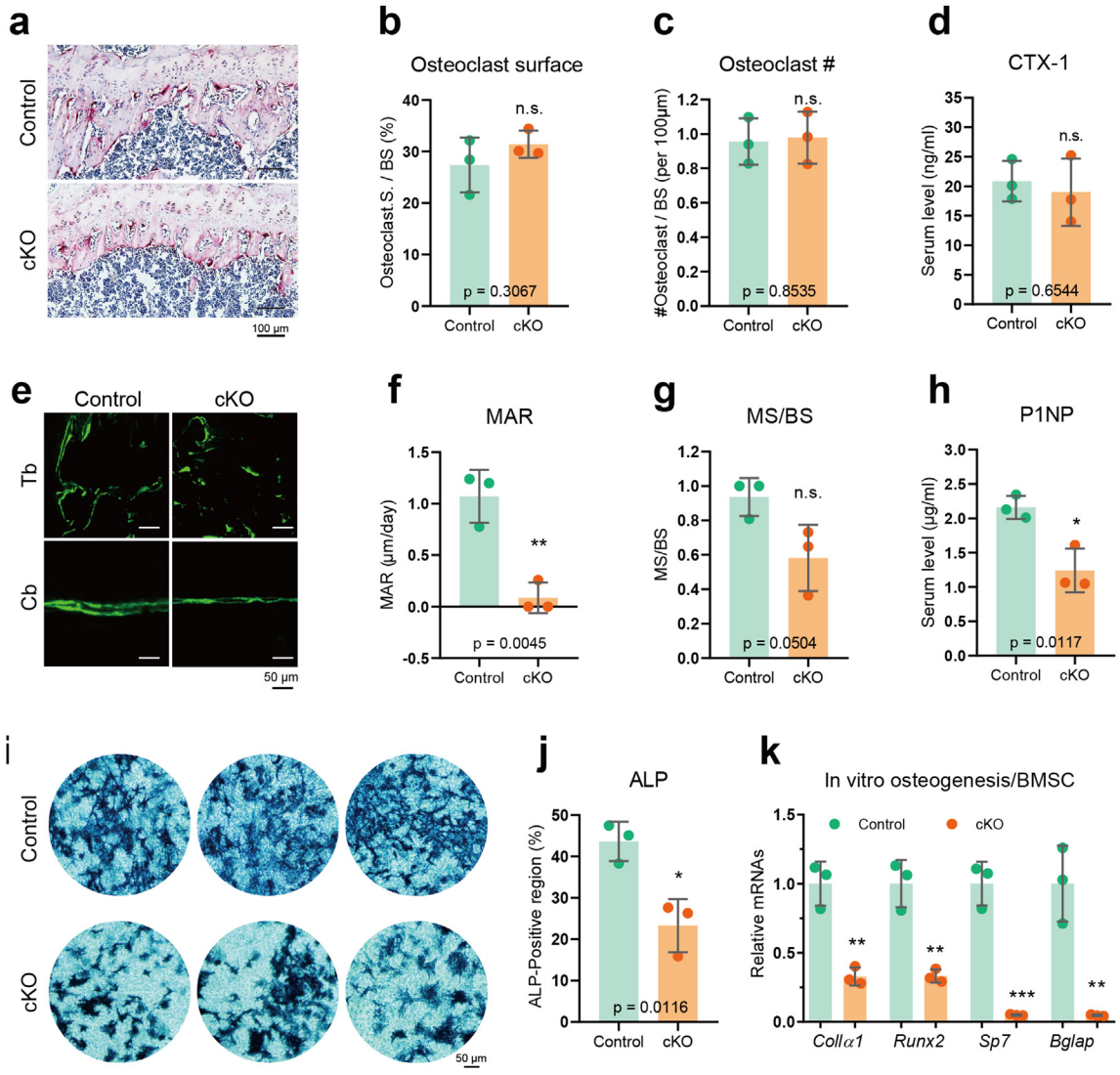

Figure 4. β1 integrin loss in osteocytes reduces bone formation without affecting osteoclast activities in bone. (**a**) Representative images of tartrate-resistant acid phosphatase (TRAP) staining from tibial sections of 4-month-old male control and cKO mice (**b–c**) Quantitative analyses of osteoclast surface and osteoclast numbers in tibial sections from TRAP staining. (**d**) Serum levels of collagen type I cross-linked C-telopeptide (CTX-1) from ELISA detection of 4-month-old male control and cKO mice. (**e**) In vivo double calcein labeling for bone formation detection in the trabecular (Tb) and cortical bone (Cb) of ulna sections of 4-month-old male control and cKO mice (**f–g**) Quantitative analyses of MAR, MS/BS for double calcein labeling results. (**h**) Serum levels of procollagen type 1 N-terminal propeptide (P1NP) from ELISA detection of 4-month-old male control and cKO mice. (**i**) Alkaline phosphatase (ALP) activity detection from BMSC osteogenic differentiation experiments (**j**) Quantitative analysis of ALP-positive regions in BMSC osteogenic differentiation experiments (**k**) The transcription of *Collα1*, *Runx2*, *Sp7* and *Bglap* were detected through quantitative PCR analysis after BMSC osteogenic differentiation. Results were collected from three biological replicates ($N = 3$) for each group. Results are expressed as mean ± standard deviation (s.d.). n. s. $p > 0.05$; *$p < 0.05$; **$p < 0.01$.

accumulation of oil droplets in cKO cultures (Fig. 5a), and the quantitative measurement (Fig. 5b) showed an average 3.82 times more oil droplets in cKO cultures compared to control cultures. Results from qPCR analyses showed that the expression levels of adipogenic differentiation genes, including those encoding peroxisome proliferator-activated receptor gamma (*Pparγ*), adiponectin (*Adipo*), adipocyte protein 2 (*Ap2*), and CCAAT/enhancer-binding protein alpha (*Cebpα*), but not *Cebpβ* and preadipocyte factor-1 (*Pref-1*), were significantly increased in cKO versus control cultures (Fig. 5c). Furthermore, we observed that a large quantity of fat was accumulated in the bone marrow of cKO tibiae, but not control mice, as demonstrated by H/E staining (Fig. 5d, g) and Perilipin immunostaining (Fig. 5e, h). Quantitative measurements further demonstrate a large number of oil droplets accumulated in the bone marrow of both trabecular and cortical bones from cKO mice (Fig. 5f, i).

3.6. β1 integrin deletion in osteocytes impairs load-induced bone formation and collagen fiber integrity

Based on our above observations of bone mass loss in load-bearing long bones (Fig. 1) and reduced FA proteins in cortical bone samples after β1 integrin deletion (Fig. 3), we wondered whether these phenotypes in cKO mice are associated with mechanical stimulations. To test the involvement of β1 integrin in osteocyte mechanotransduction, we conducted in vivo tibial loading experiments with 4-month-old male control and cKO mice. We challenged the right tibiae of experimental animals with 9.0 N cyclic mechanical compression for 2 weeks, and kept their left tibiae as intact and unload limbs. During the loading period, we monitored their tibial bone mass changes with in vivo μCT scanning on Day 1 (D1 before loading) and Day 14 (D14 after loading) (Fig. 6a). By

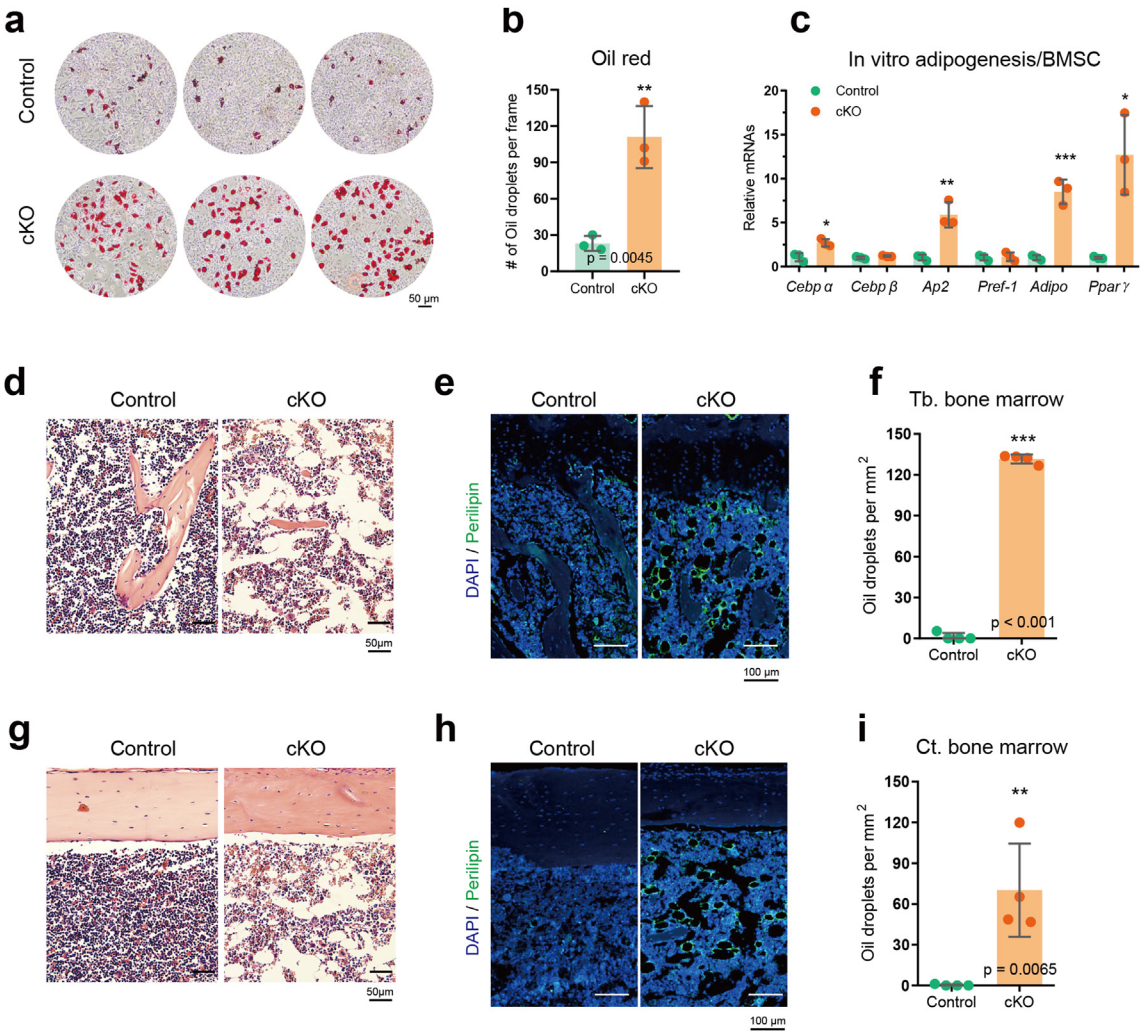

Figure 5. β1 integrin loss in osteocytes enhances BMSC adipogenic differentiation in vitro and in bone. (**a**) Oil red O staining results of adipogenic differentiation from cultured primary BMSC derived from control and cKO mice. (**b**) Quantitative analyses of numbers of oil droplets per frame in Oil red O staining results. (**c**) The transcription of *Cebpα*, *Cebpβ*, *Ap2*, *Pref-1*, *Adipo*, and *Pparγ* were detected through quantitative PCR analysis after BMSC adipogenic differentiation (**d**, **g**) H/E staining of trabecular and cortical bone and bone marrow of tibial sections from control and cKO mice (**e**, **h**) Merged immunofluorescence images of nuclei (DAPI in blue) and oil droplets (marked with Perilipin in green) in the trabecular and cortical bone sections from control and cKO tibiae (**f**, **i**) Quantitative analyses of numbers of oil droplets per 1 mm^2 in the trabecular and cortical sections from control and cKO tibiae. Results were collected from three biological replicates ($N = 3$) for each group. Results are expressed as mean ± standard deviation (s.d.). n. s. $p > 0.05$; *$p < 0.05$; **$p < 0.01$; ***$p < 0.001$.

comparing the bone mass before and after loading stimulations, we observed slight, but consistent, increases of the trabecular bone mass (yellow asterisks) and cortical bone thickness (red arrows) in control mice (Fig. 6a). However, these load-stimulated bone augmentations were lost in cKO mice (Fig. 6a). We also determined the bone formation rate with double calcein labeling experiments. As shown in Fig. 6b, bone formation was markedly enhanced by loading in the trabecular bone of tibiae from control mice, which was lost in cKO mice. Quantitative analysis focused on the ratio between load right tibiae and unload left tibiae further demonstrated significant increases of the bone mineral apposition rate (MAR) and bone formation rate per bone surface (BFR/BS) in control tibiae than those in cKO tibiae (Fig. 6c–e). Consistent with the trabecular bone results, the average increment of cortical thickness within two-week loading treatment was 6.0 ± 2.43% in control tibiae; this value was dropped to 0.57 ± 1.20% in cKO tibiae (Fig. 6f). These results suggest that mice with β1 integrin loss in osteocytes fail to properly respond to mechanical stimulation.

Considering the critical involvement of collagen fiber orientation in determination of mechanical properties, we further examined the collagen I fibers in long bones of the two genotypes with and without loading treatment through two-photon imaging. We found that mechanical loading markedly enhanced the collagen I fiber intensity in both cortical (Fig. 6g) and trabecular bones (Fig. 6h) of tibiae in control mice. In contrast, either the arbitrary intensity nor the fibrillar structure of collagen I in cKO tibiae were enhanced by loading (Fig. 6g and h). Collectively, these results demonstrate critical roles of β1 integrin in osteocytes for bone formation and collagen fiber integrity under mechanical stimulations.

4. Discussions

In the present study, we demonstrate critical roles of osteocyte β1 integrin in the control of bone mass and mediation of bone mechanotransduction. We demonstrate that mice lacking β1 integrin in osteocytes exhibit remarkable bone loss in both trabecular bone and cortical bone of load-bearing bones, including tibiae, femurs and lumbar spines, but not in non-weight-bearing calvariae. This osteopenic phenotype is associated with significant reductions of bone mechanical properties. Furthermore, we demonstrate that osteocyte β1 integrin expression is essential for normal responses of bones to mechanical loading.

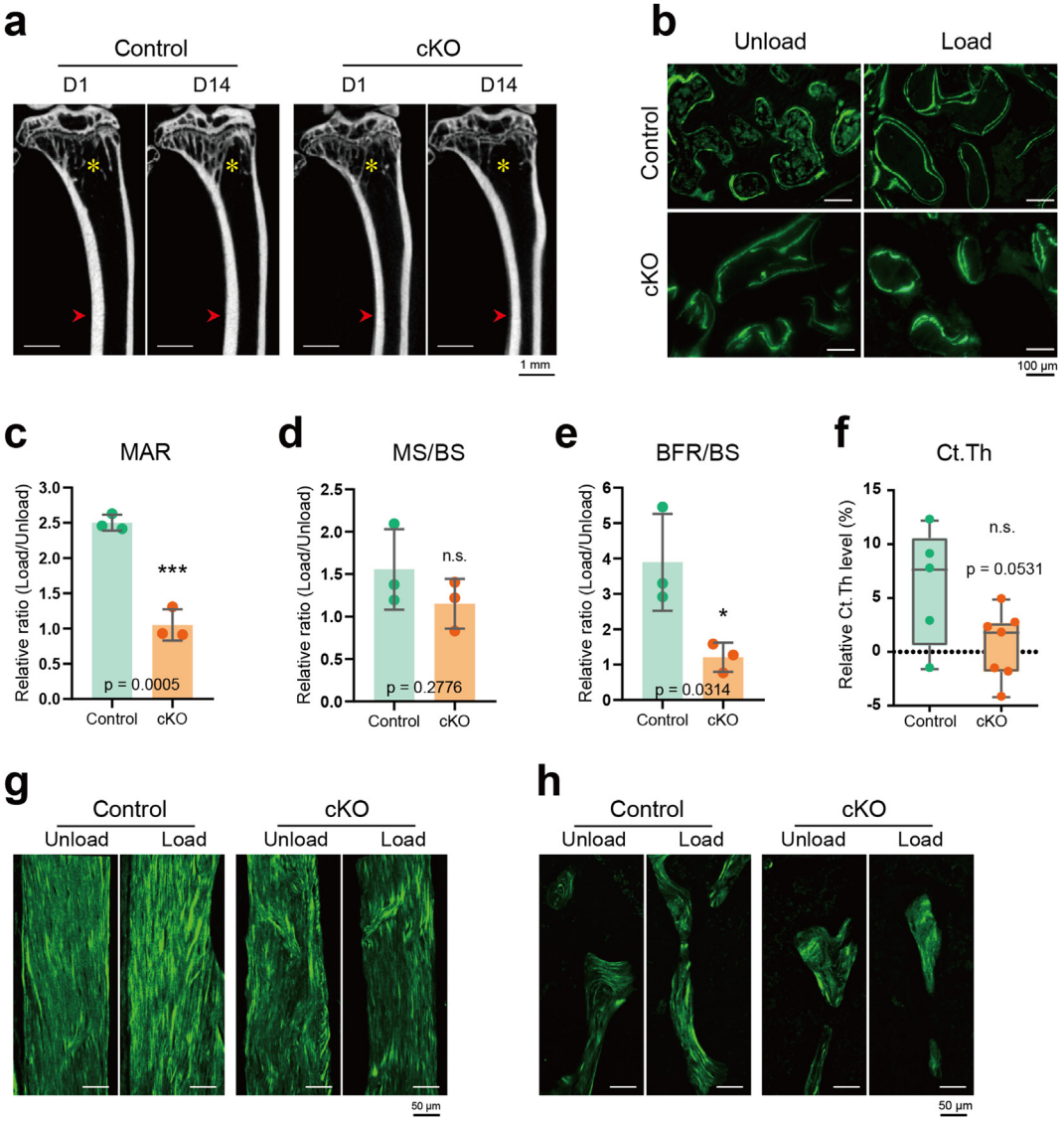

Figure 6. β1 integrin loss in osteocytes impairs load-induced bone formation and collagen fiber integrity. (**a**) In vivo μCT images on Day 1 (D1, before loading) and Day 14 (D14, after loading) of experimental control and cKO mice. Yellow asterisks indicate the trabecular bones; red arrows point to the cortical bones. (**b**) Representative double calcein labeling images for the trabecular bones from unload and load tibiae of control and cKO mice (**c**–**e**) Quantitative analyses of relative ratio between load and unload tibia in MAR, MS/BS and BFR/BS. Results were collected from three biological replicates ($N = 3$) for each group. (**f**) Relative cortical thickness changes after load compared to unload conditions. $N = 5$ for control group and $N = 7$ for cKO group (**g**–**h**) Collagen I fiber images from two-photon microscopy of unload and load cortical and trabecular bones of control and cKO tibiae. Results are expressed as mean ± standard deviation (s.d.). n. s. $p > 0.05$; *$p < 0.05$; **$p < 0.01$; ***$p < 0.001$.

We further demonstrate that β1 integrin loss in osteocytes causes bone loss through both cell-autonomous and non-cell-autonomous mechanisms in the mutant mice. On one hand, β1 integrin loss causes significant changes in osteocyte itself through cell-autonomous mechanisms. While cKO mice had no reduction of the osteocyte number in trabecular and cortical bones, they displayed altered LCS size and shape, decreased length and number of dendritic processes, as well as abnormal nuclear size and orientations in osteocytes. These alterations could negatively affect osteocyte function, including nutrient supply [49], mechanical signal transduction [21], as well as cellular communications [50]. On the other hand, osteocytes modulate bone mass and homeostasis through non-cell-autonomous mechanisms by affecting bone remodeling, i.e., the osteoclast-mediated bone resorption followed by the osteoblast-mediated bone formation. In the present study, we demonstrate that β1 integrin loss in osteocytes largely impairs osteoblast formation and function, leading to a dramatic decrease in bone formation and a low bone mass phenotype in cKO mice. Interestingly, cKO displayed reduced osteogenic, but enhanced adipogenic, differentiation in their bone marrow. Similarly, primary BMSCs derived from cKO displayed dramatic decrease in osteoblast differentiation but enhanced adipogenic differentiation in cultures. Interestingly, similar non-cell-autonomous alterations are observed in primary BMSC cultures and in bone of transgenic mice lacking other FA proteins Pinch1/2 [1] and Kindlin-2 [37] in osteocytes. It should be noted that β1 integrin loss in osteocytes does not impact osteoclast formation and bone resorption, which is similar to the results from Pinch1/2 cKO mice [1], but different from that in mice with Kindlin-2 loss in osteocytes [37]. The latter mice display reduced osteoblast, but increased osteoclast formation in bone [37]. Thus, these FA proteins in osteocytes may display different regulations of bone remodeling, and the underlying mechanisms of these differences are unclear and remain to be determined.

Previously published reports showed that deletion of β1 integrin

using the *Osteocalcin-Cre*, which is known to target both mature osteoblasts and osteocytes, caused only subtle skeletal phenotype in mice ($Itg\beta1^{Ostocalcin}$) with minor structural alternations in femurs without affecting the bone mass nor the mechanical properties [32]. Furthermore, mice with deletion of β1 integrin using the *Colla1-Cre* ($Itg\beta1^{Colla1}$), which target early and mature osteoblasts, displayed normal skeletal phenotype [51]. The phenotypic discrepancies between $Itg\beta1^{Dmp1}$ mice in current study and $Itg\beta1^{Ostocalcin}$ mice or $Itg\beta1^{Colla1}$ mice by others are probably because these *Cre* lines target different osteoblastic cell populations, i.e., *Dmp-1-Cre*, *Osteocalcin-Cre* and *Colla1-Cre* are not identical. These discrepancies could also due to potential differences in deletion efficiencies of β1 integrin in osteocytes among these *Cre* mice. Our previously published results showed that the 10-kb *Dmp1-Cre* had a significantly higher deletion efficiency in cortical osteocytes than that displayed by the 2.3-kb *Colla1-Cre* mice [37].

In the present study, we reveal a critical role of osteocyte β1 integrin in mediation of bone mechanotransduction. Our data suggest that β1 integrin exerts this key function partially through regulation of osteocyte cytoskeleton, cell orientation and ECM collagen I fiber integrity in bone, which are known to be involved in regulation of external mechanical loading and force adaptation in bone [52,53]. In addition, loss of β1 integrin further diminishes the expression of other FA-associated proteins in osteocytes, such as β3 integrin and Kindlin-2. It is worth mentioning that β1 and β3 integrins are the two major beta chains expressed in osteocytes [19]. According to published results, these two subchains display unique protein localization in osteocytes, i.e., β1 integrin was mainly located to osteocyte cell body [30], while β3 integrin was reported to be primarily expressed along osteocyte dendrites and formed FA connections with ECMs [30]. Moreover, in vitro cell culture studies demonstrate that both β1 [19] and β3 integrins [54] are necessary for propel mechanotransduction under fluid shear stress in osteocytes. It would be interesting to further examine the potential interaction and communications between these two integrin subchains in osteocytes. In the current study, we provide in vivo evidence that β1 integrin is predominantly expressed at the cell body of osteocytes and plays a crucial role in osteocyte mechanotransduction. However, detailed examinations regarding the in vivo function of β3 integrin in osteocyte mechanotransduction remains to be determined.

In summary, our study demonstrates a critical role of osteocyte β1 integrin in regulation of the cellular morphology, LCS and ECM integrity, and modulation of the bone microenvironment to maintain bone homeostasis and mediate mechanotransduction in bone. We and others showed that several FA-associated proteins, such as β1 integrin, Kindlin-2 [35], Pinch1/2 [1], and FAK [55], are essential for osteocyte-meditated bone mechanotransduction in mice. These results together emphasize a critical involvement of the FA signaling pathway in mediation of bone mechanotransduction. Our findings bring new molecular insights into osteocyte biology and may provide a potential therapeutic target for metabolic bone diseases, such as osteoporosis.

Author contributions

Study design: **GX**, **WY** and **LQ**. Study conduct: **LQ**, **TH** and **DY**. Data collection: LQ, TH, DY, YW, QY, PZ, ZL, **ZC**, **SL**, **HG**, and **ZX**. Data interpretation: **LQ**, **BT**, **QY**, **WY** and **GX**. Drafting the manuscript: LQ and GX. LQ, WY and **GX** take the responsibility for the integrity of the data analysis.

Declaration of competing interest

The authors declare that they have no competing financial interests.

Authorship

All persons who meet authorship criteria are listed as authors, and all authors certify that they have participated sufficiently in the work to take public responsibility for the content, including participation in the concept, design, analysis, writing, or revision of the manuscript. Each author certifies that this material or part thereof has not been published in another journal, that it is not currently submitted elsewhere, and that it will not be submitted elsewhere until a final decision regarding publication of the manuscript in Journal of Orthopaedic Translation has been made.

Indicate the specific contributions made by each author (list the authors' initials followed by their surnames, e.g., Y.L. Cheung). The name of each author must appear at least once in each of the three categories below.

Category 1: Conception and design of study: GX, WY, LQ; acquisition of data: LQ, TW, DY,QY, HG, ZC,ZX; analysis and/or interpretation of data: YW, PZ, ZN, SL.

Category 2: Drafting the manuscript: LQ, GX; revising the manuscript critically for important intellectual content: BT, QY, WY, GX.

Category 3: Approval of the version of the manuscript to be published (the names of all authors must be listed): LQ, TH, DY, YW, PZ, BT, QY, ZN, SL, HG, ZC, ZX. WY, GX.

Declaration of competing interest

A conflict of interest occurs when an individual's objectivity is potentially compromised by a desire for financial gain, prominence, professional advancement or a successful outcome. The Editors of the *Journal of Orthopaedic Translation* strive to ensure that what is published in the Journal is as balanced, objective and evidence-based as possible. Since it can be difficult to distinguish between an actual conflict of interest and a perceived conflict of interest, the Journal requires authors to disclose all and any potential conflicts of interest.

Section I

The authors whose names are listed immediately below certify that they have NO affiliations with or involvement in any organization or entity with any financial interest (such as honoraria; educational grants; participation in speakers' bureaus; membership, employment, consultancies, stock ownership, or other equity interest; and expert testimony or patent-licensing arrangements), or non-financial interest (such as personal or professional relationships, affiliations, knowledge or beliefs) in the subject matter or materials discussed in this manuscript.

Section II

The authors whose names are listed immediately below report the following details of affiliation or involvement in an organization or entity with a financial or non-financial interest in the subject matter or materials discussed in this manuscript. Please specify the nature of the conflict on a separate sheet of paper if the space below is inadequate.

Acknowledgements

The authors acknowledge the assistance of the Animal Center of Southern University of Science and Technology (SUSTech), Core Research Facilities of SUSTech, and the Pico Center at SUSTech. This work was supported, in part, by the National Key Research and Development Program of China Grant (2019YFA0906004), National Natural Science Foundation of China Grants (81991513, 8163066and 81870532), Guangdong Provincial Science and Technology Innovation Council Grant (2017B030301018), Nanshan District Research Project Grant (NS2021018), the Shenzhen Municipal Science and Technology Innovation Council Grant (20200925150409001) and Internal Project Grants of Huazhong University of Science and Technology Union Shenzhen Hospital (NY2021023, NY2021034, NY2021035).

Appendix A. Supplementary data

Supplementary data to this article can be found online at https://doi.org/10.1016/j.jot.2022.03.008.

References

[1] Wang Y, Yan Q, Zhao Y, Liu X, Lin S, Zhang P, et al. Focal adhesion proteins Pinch1 and Pinch2 regulate bone homeostasis in mice. JCI Insight 2019;4(22).
[2] Wu X, Qu M, Gong W, Zhou C, Lai Y, Xiao G. Kindlin-2 deletion in osteoprogenitors causes severe chondrodysplasia and low-turnover osteopenia in mice. J Orthop Translat 2022;32:41–8.
[3] Chen S, Wu X, Lai Y, Chen D, Bai X, Liu S, et al. Kindlin-2 inhibits Nlrp3 inflammasome activation in nucleus pulposus to maintain homeostasis of the intervertebral disc. Bone Res 2022;10(1):5.
[4] Wu X, Lai Y, Chen S, Zhou C, Tao C, Fu X, et al. Kindlin-2 preserves integrity of the articular cartilage to protect against osteoarthritis. Nature Aging 2022;2:332–47.
[5] Fu X, Zhou B, Yan Q, Tao C, Qin L, Wu X, et al. Kindlin-2 regulates skeletal homeostasis by modulating PTH1R in mice. Signal Transduct Targeted Ther 2020;5(1):297.
[6] Harburger DS, Calderwood DA. Integrin signalling at a glance. J Cell Sci 2009;122(2):159–63.
[7] Zaidel-Bar R, Itzkovitz S, Ma'ayan A, Iyengar R, Geiger B. Functional atlas of the integrin adhesome. Nat Cell Biol 2007;9(8):858–67.
[8] Geiger B, Spatz JP, Bershadsky AD. Environmental sensing through focal adhesions. Nat Rev Mol Cell Biol 2009;10(1):21–33.
[9] Howe GA, Addison CL. β1 integrin: an emerging player in the modulation of tumorigenesis and response to therapy. Cell Adhes Migrat 2012;6(2):71–7.
[10] Molè MA, Weberling A, Fässler R, Campbell A, Fishel S, Zernicka-Goetz M. Integrin β1 coordinates survival and morphogenesis of the embryonic lineage upon implantation and pluripotency transition. Cell Rep 2021;34(10):108834.
[11] Fujioka T, Kaneko N, Ajioka I, Nakaguchi K, Omata T, Ohba H, et al. β1 integrin signaling promotes neuronal migration along vascular scaffolds in the post-stroke brain. EBioMedicine 2017;16:195–203.
[12] Desgrosellier JS, Cheresh DA. Integrins in cancer: biological implications and therapeutic opportunities. Nat Rev Cancer 2010;10(1):9–22.
[13] Slack RJ, Macdonald SJF, Roper JA, Jenkins RG, Hatley RJD. Emerging therapeutic opportunities for integrin inhibitors. Nat Rev Drug Discov 2021;21:60–78.
[14] Hughes DE, Salter DM, Dedhar S, Simpson R. Integrin expression in human bone. J Bone Miner Res 1993;8(5):527–33.
[15] Duong LT, Lakkakorpi P, Nakamura I, Rodan GA. Integrins and signaling in osteoclast function. Matrix Biol 2000;19(2):97–105.
[16] Ren J, Jin P, Sabatino M, Balakumaran A, Feng J, Kuznetsov SA, et al. Global transcriptome analysis of human bone marrow stromal cells (BMSC) reveals proliferative, mobile and interactive cells that produce abundant extracellular matrix proteins, some of which may affect BMSC potency. Cytotherapy 2011;13(6):661–74.
[17] Fu X, Liu G, Halim A, Ju Y, Luo Q, Song G. Mesenchymal stem cell migration and tissue repair. Cells 2019;8(8):784.
[18] Popov C, Radic T, Haasters F, Prall WC, Aszodi A, Gullberg D, et al. Integrins α2β1 and α11β1 regulate the survival of mesenchymal stem cells on collagen I. Cell Death Dis 2011;2(7):e186.
[19] Geoghegan IP, Hoey DA, McNamara LM. Integrins in osteocyte biology and mechanotransduction. Curr Osteoporos Rep 2019;17(4):195–206.
[20] Marie PJ, Haÿ E, Saidak Z. Integrin and cadherin signaling in bone: role and potential therapeutic targets. Trends in Endocrinology & Metabolism 2014;25(11):567–75.
[21] Qin L, Liu W, Cao H, Xiao G. Molecular mechanosensors in osteocytes. Bone Research 2020;8(1):23.
[22] Raducanu A, Hunziker EB, Drosse I, Aszódi A. Beta1 integrin deficiency results in multiple abnormalities of the knee joint. J Biol Chem 2009;284(35):23780–92.
[23] Bonewald LF. The amazing osteocyte. J Bone Miner Res 2011;26(2):229–38.
[24] Dallas SL, Prideaux M, Bonewald LF. The osteocyte: an endocrine cell … and more. Endocr Rev 2013;34(5):658–90.
[25] Han Y, You X, Xing W, Zhang Z, Zou W. Paracrine and endocrine actions of bone-the functions of secretory proteins from osteoblasts, osteocytes, and osteoclasts. Bone Res 2018;6:16.
[26] Schaffler MB, Cheung WY, Majeska R, Kennedy O. Osteocytes: master orchestrators of bone. Calcif Tissue Int 2014;94(1):5–24.
[27] Qin L, He T, Chen S, Yang D, Yi W, Cao H, et al. Roles of mechanosensitive channel Piezo1/2 proteins in skeleton and other tissues. Bone Research 2021;9(1):44.
[28] Li MCM, Chow SKH, Wong RMY, Qin L, Cheung WH. The role of osteocytes-specific molecular mechanism in regulation of mechanotransduction – a systematic review. Journal of Orthopaedic Translation 2021;29:1–9.
[29] Guo E. Calcium-dependent actomyosin contractility in osteocytes under mechanical loading. Journal of Orthopaedic Translation 2014;2(4):199.
[30] McNamara LM, Majeska RJ, Weinbaum S, Friedrich V, Schaffler MB. Attachment of osteocyte cell processes to the bone matrix. Anat Rec 2009;292(3):355–63.
[31] Cabahug-Zuckerman P, Stout RF Jr, Majeska RJ, Thi MM, Spray DC, Weinbaum S, et al. Potential role for a specialized β(3) integrin-based structure on osteocyte processes in bone mechanosensation. J Orthop Res 2018;36(2):642–52.
[32] Shekaran A, Shoemaker JT, Kavanaugh TE, Lin AS, LaPlaca MC, Fan Y, et al. The effect of conditional inactivation of beta 1 integrins using twist 2 Cre, Osterix Cre and osteocalcin Cre lines on skeletal phenotype. Bone 2014;68:131–41.
[33] Zimmerman D, Jin F, Leboy P, Hardy S, Damsky C. Impaired bone formation in transgenic mice resulting from altered integrin function in osteoblasts. Dev Biol 2000;220(1):2–15.
[34] Lu Y, Xie Y, Zhang S, Dusevich V, Bonewald LF, Feng JQ. DMP1-targeted Cre expression in odontoblasts and osteocytes. J Dent Res 2007;86(4):320–5.
[35] Qin L, Fu X, Ma J, Lin M, Zhang P, Wang Y, et al. Kindlin-2 mediates mechanotransduction in bone by regulating expression of Sclerostin in osteocytes. Commun Biol 2021;4(1):402.
[36] Wu C, Jiao H, Lai Y, Zheng W, Chen K, Qu H, et al. Kindlin-2 controls TGF-β signalling and Sox9 expression to regulate chondrogenesis. Nat Commun 2015;6:7531.
[37] Cao H, Yan Q, Wang D, Lai Y, Zhou B, Zhang Q, et al. Focal adhesion protein Kindlin-2 regulates bone homeostasis in mice. Bone Res 2020;8:2.
[38] Ren Y, Liu Y, Feng JQ. A novel way for qualitative and quantitative Analyses of morphologic changes osteocytes in health and disease. Journal of Orthopaedic Translation 2014;2(4):197–8.
[39] Gao H, Guo Y, Yan Q, Yang W, Li R, Lin S, et al. Lipoatrophy and metabolic disturbance in mice with adipose-specific deletion of kindlin-2. JCI Insight 2019;4(13).
[40] Gao H, Zhong Y, Ding Z, Lin S, Hou X, Tang W, et al. Pinch loss ameliorates obesity, glucose intolerance, and fatty liver by modulating adipocyte apoptosis in mice. Diabetes 2021;70(11):2492–505.
[41] Zhu K, Lai Y, Bai X, Liu C, Yan Q, Ma L, et al. Kindlin-2 modulates MafA and β-catenin expression to regulate β-cell function and mass in mice. Nat Commun 2020;11(1):484.
[42] Gao H, Zhou L, Zhong Y, Ding Z, Lin S, Hou X, et al. Kindlin-2 haploinsufficiency protects against fatty liver by targeting Foxo1 in mice. Nat Commun 2022;13(1):1025.
[43] Lei Y, Fu X, Li P, Lin S, Yan Q, Lai Y, et al. LIM domain proteins Pinch1/2 regulate chondrogenesis and bone mass in mice. Bone Res 2020;8:37.
[44] Morgan EF, Unnikrisnan GU, Hussein AI. Bone mechanical properties in healthy and diseased states. Annu Rev Biomed Eng 2018;20:119–43.
[45] Unal M, Creecy A, Nyman JS. The role of matrix composition in the mechanical behavior of bone. Curr Osteoporos Rep 2018;16(3):205–15.
[46] Ibrahim A, Magliulo N, Groben J, Padilla A, Akbik F, Abdel Hamid Z. Hardness, an important indicator of bone quality, and the role of collagen in bone hardness. J Funct Biomater 2020;11(4).
[47] Viguet-Carrin S, Garnero P, Delmas PD. The role of collagen in bone strength. Osteoporos Int 2006;17(3):319–36.
[48] Zoumi A, Yeh A, Tromberg BJ. Imaging cells and extracellular matrix in vivo by using second-harmonic generation and two-photon excited fluorescence. Proc Natl Acad Sci U S A 2002;99(17):11014–9.
[49] Lai X, Price C, Modla S, Thompson WR, Caplan J, Kirn-Safran CB, et al. The dependences of osteocyte network on bone compartment, age, and disease. Bone Research 2015;3(1):15009.
[50] Wang JS, Kamath T, Mazur CM, Mirzamohammadi F, Rotter D, Hojo H, et al. Control of osteocyte dendrite formation by Sp7 and its target gene osteocrin. Nat Commun 2021;12(1):6271.
[51] Litzenberger JB, Tang WJ, Castillo AB, Jacobs CR. Deletion of β1 integrins from cortical osteocytes reduces load-induced bone formation. Cell Mol Bioeng 2009;2(3):416–24.
[52] van Oers RF, Wang H, Bacabac RG. Osteocyte shape and mechanical loading. Curr Osteoporos Rep 2015;13(2):61–6.
[53] Wu V, van Oers RFM, Schulten EAJM, Helder MN, Bacabac RG, Klein-Nulend J. Osteocyte morphology and orientation in relation to strain in the jaw bone. Int J Oral Sci 2018;10(1):2.
[54] Haugh MG, Vaughan TJ, McNamara LM. The role of integrin α(V)β(3) in osteocyte mechanotransduction. J Mech Behav Biomed Mater 2015;42:67–75.
[55] Sato T, Verma S, Andrade CDC, Omeara M, Campbell N, Wang JS, et al. A FAK/HDAC5 signaling axis controls osteocyte mechanotransduction. Nat Commun 2020;11(1):3282.